Available online at www.sciencedirect.com
SCIENCE DIRECT®
Surface Science 595 (2005) 64–72
SURFACE SCIENCE
www.elsevier.com/locate/susc

The effects of buffer structure in buffer-layer-assisted growth: Grain boundaries, grooves, and pattern transfer

J.S. Palmer, V.N. Antonov, A.S. Bhatti [1], P. Swaminathan, P.S. Waggoner, J.H. Weaver *

Department of Materials Science and Engineering, University of Illinois at Urbana-Champaign, Urbana, IL 61801, USA
Department of Physics, University of Illinois at Urbana-Champaign, Urbana, IL 61801, USA
Frederick Seitz Materials Research Laboratory, University of Illinois at Urbana-Champaign, Urbana, IL 61801, USA

Received 27 May 2005; accepted for publication 30 July 2005
Available online 18 August 2005

Abstract

Rare gas thin solid films have been used to create a wide range of nanostructures through buffer-layer-assisted growth. This paper examines effects related to the microstructure of the buffer layer and demonstrates that those effects can be used to produce nanostructures with different spatial distributions. We show that ~100 ML thick Xe films form large columnar grains through secondary grain growth when condensed on amorphous substrates at 15–40 K. The grains grow to reach diameters exceeding 30 times their film thickness. Moreover, surface grooving occurs where the grain boundaries intersect the buffer surface. The deposition of Au atoms onto these surfaces produces clusters, and warm-up induces cluster diffusion and aggregation during buffer desorption before delivery to the surface. Transmission electron microscopy results show that the grooves capture the mobile clusters and concentrate them in a fashion analogous to the capture of agitated grains of sand on a patterned surface. The grain boundaries and their grooves then offer a way to vary the cluster distribution on the surface and to print by pattern transfer using nanoscale particles of a material of choice.

Keywords: Buffer-layer-assisted growth; Grain boundaries; Noble gases; Growth; Electron microscopy

1. Introduction

Cluster-assembly on surfaces is viewed as a promising technique for building devices and device arrays at the nanoscale [1]. An important issue for such assembly is the interaction between the clusters and the surface, since these interactions

* Corresponding author. Address: Department of Materials Science and Engineering, University of Illinois at Urbana-Champaign, Urbana, IL 61801, USA. Tel.: +1 217 244 3528; fax: +1 217 333 2736.
E-mail address: jhweaver@uiuc.edu (J.H. Weaver).
[1] Present address: Department of Physics, COMSATS Institute of Information Technology, Sector H—8/1, Islamabad, Pakistan.

0039-6028/$ - see front matter © 2005 Elsevier B.V. All rights reserved.
doi:10.1016/j.susc.2005.07.039

impose severe restrictions on both cluster formation and cluster mobility. A novel and robust way of circumventing those restrictions is a technique introduced by Waddill et al. [2] that is now known as buffer-layer-assisted growth or BLAG [3]. In BLAG, atoms of the material of choice are vapor-deposited onto thin layers of inert gas solids that have been grown at 20–50 K on any substrate [2–7]. Three-dimensional clustering occurs on the buffer, and subsequent warm-up sublimes the buffer so that the clusters are delivered to the pristine surface in the ultimate of soft-landing. BLAG makes it possible to prepare a wide range of nanostructure/support systems that cannot be formed by conventional deposition techniques, e.g. Ge clusters on Si without a wetting layer [8]. Moreover, the density of the nanostructures produced with BLAG can be varied over more than two orders of magnitude by changing the buffer thickness; the amount of material deposited makes it possible to produce compact or ramified clusters derived from tens to many hundreds of thousands of atoms [3,9,10].

Several recent BLAG studies have concentrated on the interaction of the clusters and the buffer. One showed that ramified structures were formed that had fractal dimensions consistent with diffusion-limited cluster–cluster aggregation (DLCCA) models [9,10]. Another showed that particle diffusion proceeds through slip at the highly incommensurate particle-buffer interface, and that slip is activated by multi-phonon processes as the buffer warms and desorbs [11,12]. An extension of BLAG to solid molecular CO_2 has revealed similar activation for diffusion and has shown the feasibility of using such layers for nanoparticle synthesis [13].

In this paper, we address issues related to the microstructure of the buffer layer and its effect on cluster aggregation. We show that rare gas thin films are made up of large columnar grains with low energy surfaces and that grain formation occurs through secondary grain growth. Groove formation at the grain boundaries, which is well-known for metals at elevated temperatures, leads to the capture of clusters when their motion is activated during warm-up and buffer desorption. The cluster distribution then reflects the groove patterns, and the distribution of clusters on the surface represents a print of those patterns.

2. Experiment

The samples were grown in an ultrahigh-vacuum (UHV) chamber with a typical base pressure below 1×10^{-10} Torr. The substrates were 20–30-nm-thick amorphous carbon (a-C) and amorphous SiO_x foil supported on copper grids obtained from Electron Microscopy Sciences and SPI Supplies. Those foils were formed by vapor condensation on thin supported soap films. After growth, the soap films were dissolved and the floating foils could be suspended over copper grids. The substrates were used as received without further preparation. A resistive heater mounted between the substrate and the cold head of a closed-cycle He refrigerator was used to control the sample temperature in the range between 15 and 60 K. The temperature was measured with a AuFe-Chromel thermocouple. Xenon gas was introduced into the chamber through a precision leak valve to condense the buffer layer. The pressure was maintained at 1×10^{-6} Torr, and it was monitored with an ion gauge, corrected for Xe sensitivity. The buffer growth rate was estimated from the number of incident atoms per unit time per unit area, namely $I = p/(2\pi mkT)^{1/2}$, where p is the Xe partial pressure, m is the mass of a Xe atom, T is the ambient temperature, and the sticking coefficient was assumed to be unity. The layer thicknesses are given in monolayers where 1 ML of Xe(1 1 1) results from a 3.5 Langmuir exposure and corresponds to an atom density of $6 \times 10^{14}\,\mathrm{cm}^{-3}$. Gold atoms were evaporated onto the buffer layer from a tungsten basket. The impinging Au atoms were sufficiently mobile that they could form clusters, a process favored by weak bonding with the rare gas solid. Cluster diffusion occurred as the samples were warmed through the 75–85 K window and the Xe sublimed.

Characterization of the samples was done at room temperature after their transfer to a Philips CM12 120-kV transmission electron microscope (TEM). Imaging was done in the bright-field

mode, keeping the beam intensity low to avoid significant changes in nanostructure morphology. The samples were stable when stored in air, and there was no evidence of coarsening.

3. Initial nucleation and secondary grain growth

The adsorption of Xe on a cold substrate and first layer island nucleation is governed not only by temperature and deposition rates but also by the substrate structure and its cleanliness. Xenon adsorption produces layer by layer growth with a compact (1 1 1) structure on the basal plane of clean graphite where there is a good lattice match [14]. However, the presence of adsorbates significantly alters this growth process, and multilayer Xe islands form on graphite substrates that have not been heat treated in UHV [14]. Since our substrates were air exposed and processed in an aqueous environment with no in vacuo cleaning, we expect adsorbates that would affect first-layer sticking, wetting, and island growth. Their amorphous nature could also contribute to deviations from close-packed ordering [14]. Subsequent condensation beyond the first layer should result in island thickening and expansion to create a polycrystalline film with differently oriented grains, the details of which would reflect the growth temperature.

To gain insight into the initial nucleation density for the buffer layer, we exposed a-C and SiO_x surfaces to enough Xe to grow a 6 ML thick film at 34 K. This thickness was chosen so that we could determine whether there was multilayer island growth prior to the formation of a continuous film. Exploiting the capabilities of BLAG, we reasoned that inhomogeneities in the Xe layer would be reflected in the size and distribution of clusters that would form following the deposition of 3 Å of Au. In particular, Au clusters would form on the multilayer islands, and they would diffuse and aggregate during buffer desorption, as usual in BLAG. The Xe island shapes could be deduced from the cluster pattern after delivery to the substrate.

Fig. 1(a) and (b) show a bimodal size distribution for Au clusters on both a-C and SiO_x. The background of the images has been altered to identify regions where Xe had been present. The darker regions with smaller clusters represent areas where Au was delivered directly to the unbuffered substrate (portions that had not been wet by the Xe). In those areas, clustering would occur when the samples warmed to room temperature and Au diffusion was activated, as with conventional physical vapor deposition onto a-C or SiO_x [15]. Larger Au clusters were formed on the Xe islands (lighter regions), where the cluster densities and sizes are consistent with those grown on uniform

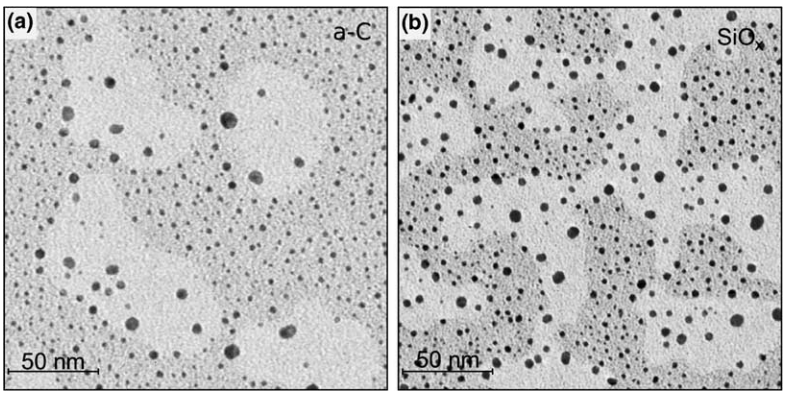

Fig. 1. TEM micrographs of clusters formed by depositing 3 Å Au on 6 ML of Xe condensed at 34 K on a-C and SiO_x substrates after heating to remove the Xe buffer layer. The bimodal cluster size distribution reflects the nonuniformity of the buffer layer that grows on the air-exposed substrates. The image backgrounds have been altered to enhance the contrast between the Xe-covered (light) and bare (dark) regions: (a) on a-C, the Xe islands covered 33% of the surface, and they had an initial density of $\sim 1 \times 10^{10}$ cm^{-2} and (b) on SiO_x, the island coverage was 46%, and the initial density was $\sim 2 \times 10^{10}$ cm^{-2}.

Xe films with thickness greater than 10 ML condensed at 20 K. (Exact comparison cannot be made because many of the clusters have diffused to the island edges where their subsequent motion differs from that on a uniform film.) On a-C, the initial Xe island density is $\sim 1.3 \times 10^{10}\,\mathrm{cm}^{-2}$ and the islands covered ~33% of the surface. On SiO_x, we estimate a slightly higher initial island density of $\sim 2.0 \times 10^{10}\,\mathrm{cm}^{-2}$ (assuming some islands had started to coalesce) and that ~46% of the surface was covered. These images reflect differences in Xe atom sticking coefficients, mobility, and nucleation. Most significantly, they show that the initial islands are small and island center-to-center distances are 50–100 nm.

The question that arises from Fig. 1 involves how the buffer layer evolves as more Xe is condensed. TEM observations of vapor-deposited films of Xe on a-C substrates have shown columnar grains with (1 1 1) surfaces [16]. To gain insights into the structure of thicker BLAG layers, we took advantage of a process that is well-known from the metals literature, namely that grooves will form when a grain boundary intersects the surface. This process is discussed in the next section, but the possible existence of grooves suggested that they might act as traps for diffusing clusters and that the Xe grain boundary patterns could be transferred to the buffered surface.

To determine whether pattern transfer could be observed, we grew clusters by depositing 5 Å of Au on a 95 ML thick Xe buffer condensed at 40 K on a-C. This thickness was chosen because thinner films allow too little cluster diffusion and thicker films allow too much aggregation for effective patterning. Fig. 2(a) is a low resolution TEM micrograph that has been digitally blurred using Gaussian-weighted pixel averaging. The dark lines correspond to enhanced cluster densities, identifying where the Xe grain boundaries were prior to desorption. Fig. 2(b) is an unprocessed micrograph of the same area where the grain boundary positions deduced from Fig. 2(a) are overlaid. Fig. 2(c) shows a higher resolution image of the boxed area, revealing how the clusters are distributed relative to the Xe grain boundaries. The lines mark the grain boundary region as revealed in Fig. 2(a). The Au cluster density is $4.8 \times 10^{9}\,\mathrm{cm}^{-2}$, and the clusters are ramified with a fractal radius of ~20 nm, as observed on similar samples prepared at 20 K [11]. Note that under normal imaging, the increased concentration of clusters at the grain boundary would not be noticed. Now, however, it is possible to determine a typical grain size of 2.6 μm.

The grain density in Fig. 2 is over three orders of magnitude less than the initial island density of Fig. 1. Moreover, the width-to-height ratios

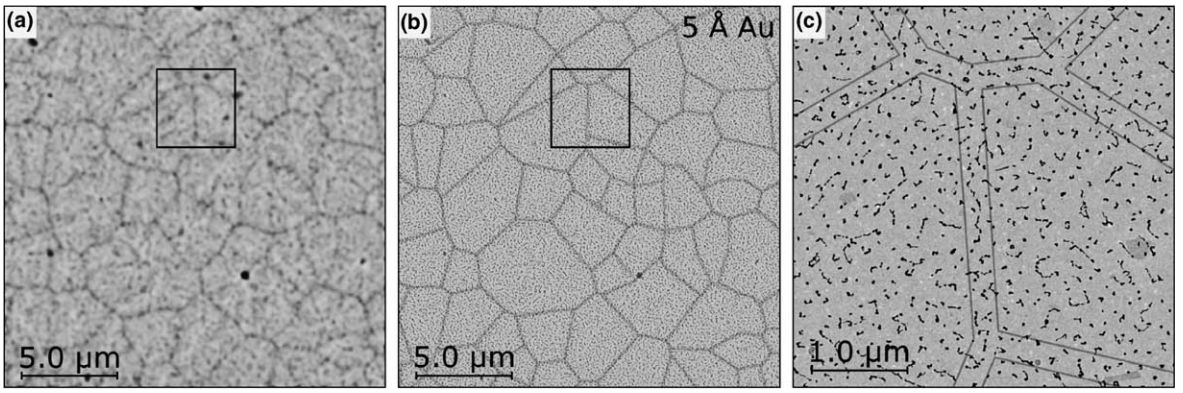

Fig. 2. (a) A low magnification bright field TEM micrograph of particles grown from a deposition of 5 Å Au on 95 ML of Xe condensed at 40 K. The image was digitally blurred using Gaussian-weighted pixel averaging to reveal cluster accumulation in regions where there had been grain boundaries and grooves in the Xe film, (b) the same image as in (a) prior to blurring. The lines were drawn to show the grain boundary network deduced from (a) and (c) a higher resolution image of the square area reveals how the clusters are distributed relative to the marked grain boundary region.

are much larger than expected from primary or normal grain growth where grain widths are limited to a few times the film thickness [17]. The development of such large grains can be understood in terms of secondary or abnormal grain growth. Primary grain growth is driven by a reduction in grain boundary energy and results in films with a log-normal grain size distribution. In secondary grain growth, so called abnormal grains grow at a much higher rate than normal grains, leading to a bimodal size distribution. In thin films, secondary growth is driven by reduction in surface and interface energies rather than grain boundary energies. The sketch in Fig. 3(a) depicts a large abnormal grain growing and consuming surrounding grains that have higher surface and interface energies [17]. The abnormal grains will continue to grow until they impact one another and the grains again develop a monomodal size distribution. At this point, grains are no longer expected to grow because the driving force for secondary growth no longer exists and that for primary growth is insignificant [17].

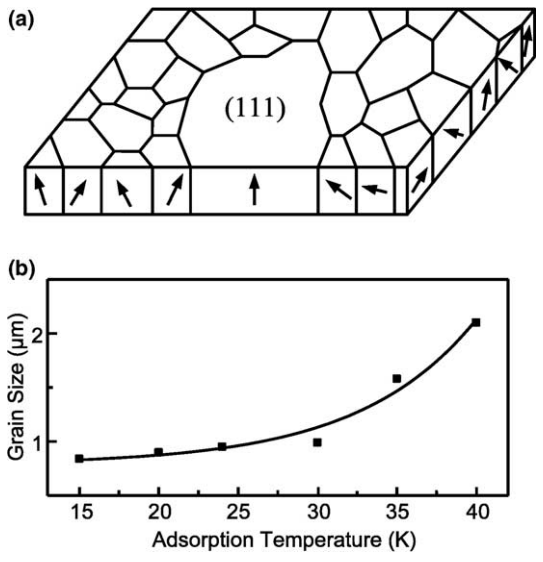

Fig. 3. (a) A schematic of secondary grain growth. The arrows signify that the grains have many different orientations. Grains with lower surface and interface energies grow at the expense of their neighbors, thus causing a bimodal grain size distribution and (b) the observed dependence of the final grain size on buffer condensation temperature as deduced from results like that in Fig. 2(b).

Although referred to as secondary grain growth, we suspect that structural changes occur during Xe film growth. Wong et al. observed secondary growth in Au thin films deposited on SiO_x at room temperature, i.e. at ~22% of the melting temperature [18]. Following the deposition of 10 nm of Au, they reported islands with large open areas that are qualitatively similar to those deduced for Xe in Fig. 1(b). A polycrystalline film formed upon further Au deposition, with randomly-oriented grains with sizes on the order of the film thickness. Significantly, the onset of secondary growth was observed as soon as the film was continuous, and Wong et al. reported that the (1 1 1) grains increased rapidly in size with continued deposition. We envision a similar growth sequence for Xe films condensed at ~34 K. With condensation beyond that of Fig. 1, a polycrystalline film would develop, and the grains would grow through both primary and secondary pathways until the surface is all (1 1 1). As predicted, we observe that the grain sizes are stagnant after secondary growth was completed, even with annealing at 45 K [19].

Thompson presented a model for secondary thin film growth that links final grain sizes to the initial grain structure [20]. The model predicts that the final grain sizes increase with film thickness and that they are strongly affected by the initial grain sizes and orientations. During secondary growth, the lower-energy abnormal grains consume the surrounding grains. The larger the incorporated grains are, the larger the final grains will be. In addition, the lower the fraction of low-energy-oriented grains, the greater the number of initial grains that will be incorporated into a single grain, and hence the final grains will be bigger. To investigate whether this model would be applicable to thin Xe films, we varied the condensation rate and temperature, expecting that both would influence the initial grain sizes and orientations. Interestingly, variations in the growth rate from 0.03 ML s^{-1} to 3 ML s^{-1} at 15 K had a negligible effect on the grain size. As summarized in Fig. 3(b), increasing the condensation temperature from 15 K to 34 K only increased the average

grain size 85% from 0.85 μm to 1.58 μm. The reason for the weak dependence on temperature (or condensation rate) is that the initial grains are larger for higher temperatures, but a larger fraction of the grains are initially (1 1 1) oriented. With more abnormal (well-oriented) grains, fewer grains will be consumed, and the final structure will be characterized by smaller grains. The effects of initial size and initial orientation partially cancel one another, resulting in weak dependence of the grain size on the adsorption rate or growth temperature.

4. Grain boundary grooving and groove evolution

It is well-known that surfaces of polycrystalline materials are roughened and grooves form where grain boundaries intersect the surface. A quantitative continuum theory of thermal grain boundary grooving was developed by Mullins [21]. As depicted in Fig. 4 for a film-vacuum interface, thermal grooves introduce long range roughening and involve the diffusion of buffer material from grain boundary regions toward the center of the grains [22]. Grooving is driven by thermodynamics as the affected regions seek to lower their energies. Their formation is responsible for the patterning of Fig. 2.

The equilibrium structure near a grain boundary is dictated by the balance between the surface free energies f_s and the grain boundary free energy f_{gb} at the intersection line,

$$f_{gb} = 2f_s \sin\alpha, \tag{1}$$

where, for simplicity, the surfaces and f_s are assumed to be symmetric across the boundary and the angle α is defined in Fig. 4. Surface diffusion and/or evaporation–condensation processes would then drive the flat surface ($\alpha = 0$) to form a groove with the angle α determined by the free energies.

The ejected material would accumulate into ridges on either side of the groove, but the ridges would be thermodynamically unstable and dissipate through adatom diffusion. This diffusion would effectively lower α, forcing further deepening of the groove to restore the equilibrium angle. The groove depth d would then increase with time, and Mullins derived a $d \sim (\text{time})^{1/4}$ dependence for surface-diffusion-mediated processes. Significantly, the groove shape would remain independent of depth since it is determined by the equilibrium value of α. Grooving would halt when the curvature was constant over the whole grain surface because conservation of mass would require increasing the angle α for continued grooving. Of course, the groove could reach the surface before equilibrium is reached, depending on the angle α, the initial grain thickness, and the grain diameter [23].

In order to determine whether the grain boundary grooves were, indeed, deepening with time, we grew Kr thin films and deposited Au onto them. Krypton is superior to Xe for such studies because it has a lower cohesive energy, a much higher surface diffusivity at 20 K, and a faster rate of grooving. Investigations of Au nanostructures produced using BLAG on freshly condensed Kr showed densities and distributions that were qualitatively similar to those grown on Xe [11]. However, when a 95 ML thick Kr buffer with Au clusters was aged for 26 h at 20 K, the result was a bimodal cluster size distribution, with channels of high-density, small clusters surrounding regions with larger Au aggregates.

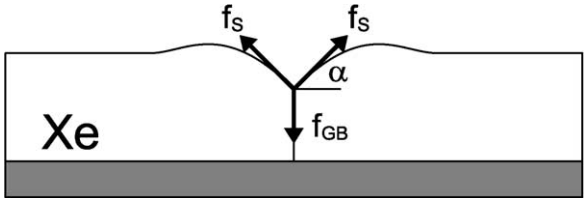

Fig. 4. A schematic of thermal grooving of a grain boundary as described in Ref. [21]. Grooves form at the intersection of a grain boundary with the vacuum due to the imbalance of the interface free energies. The angle of the groove α is defined by the interface energies, and it remains constant as the groove deepens.

The TEM images indicate that the grooves deepened and reached the surface, and that the film dewets the surface. In the regions of deepening grooves, Au clusters that had nucleated on the Kr were gently delivered to the substrate. In contrast, clusters that had nucleated far from the grooves diffused and aggregated into larger structures, as usual. The density of the large-cluster regions where Kr was present is $2.7 \times 10^8\,\mathrm{cm}^{-2}$, about two orders of magnitude lower than the initial island density of Fig. 1, indicating the Kr film also experienced secondary grain growth.

Prior to the formation of grooves, the continuous Kr film was stabilized by kinetics. Grooving reduced the barrier for dewetting by thinning the film and exposing the surface. Thus, the surface conditions that initially gave rise to inhomogeneous island growth (Fig. 1), but which were subsequently overgrown and buried during primary and secondary growth, were again important and lead to dewetting around the grains.

5. Pattern transfer with grooves

The fact that the grain boundary positions become apparent upon blurring an image reveals the higher density of cluster material near the grain boundaries. Cluster diffusion is driven by multiphonon processes as the buffer layer warms, and diffusivity scales inversely with the cluster-buffer contact area [11,12]. Diffusing clusters could not cross a groove without significantly decreasing their contact area and a cluster in a groove would have an increased contact area as it touches both sides of the groove. These contact area considerations prevent clusters from diffusing across or away from the grooves and allow them to diffuse along the groove.

To learn more about grain boundary pattern transfer, we varied the amount of Au deposited on Xe buffers so as to vary the cluster density and size distribution. Fig. 5(a)–(c) show the effects of depositing 0.7, 2, and 3.5 Å of Au on a 95 ML Xe buffer condensed at 34 K on SiO_x. The effect of the grain boundaries is particularly evident in Fig. 5(a). A reduction in the amount of Au deposited resulted in smaller cluster sizes, reduced surface coverage, and much more accumulation at the grain boundary. Increasing the amount of Au causes the clusters to be more uniformly distributed because of their reduced diffusion length. For the sample in Fig. 5(a), the average coverage was 1.5% and, significantly, 90% of the clusters were observed within 100 nm of the grain boundary. This results in a web-like pattern of clusters separated by large cluster-free regions.

In order to quantify the accumulation of clusters, we measured the average coverage as a function of the distance from the grain boundary. Fig. 6 shows the results of averaging along many grain boundaries for the samples in Fig. 5. The

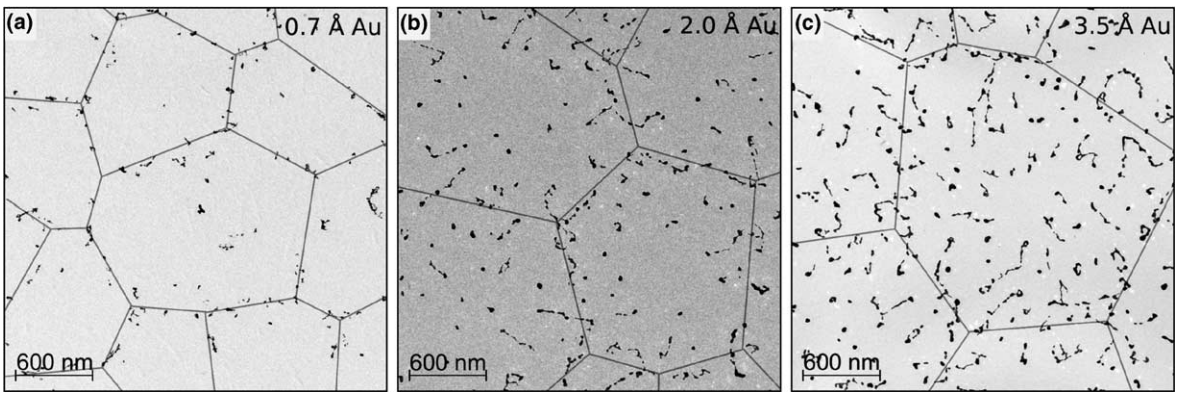

Fig. 5. The cluster distributions for (a) 0.7, (b) 2 and (c) 3.5 Å of Au deposited on 95 ML Xe buffers condensed at 34 K. The surface coverages were 1.5%, 2.7% and 6.0%. The cluster diffusion length is largest for smaller clusters and for lower coverage. This diffusion leads to cluster trapping at the grooves and pattern transfer when the buffer desorbs.

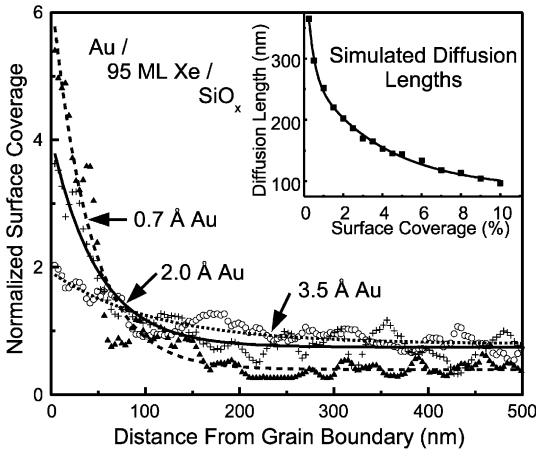

Fig. 6. Surface coverage as a function of distance from a Xe grain boundary deduced from Fig. 5. The profiles are normalized to the average coverage of the sample. The clusters are more uniformly distributed across the sample as the coverage or amount of Au deposited increases. The inset shows the cluster diffusion length determined by DLCCA Monte Carlo simulations after a fixed amount of time. The diffusion lengths fall off exponentially as the surface coverage is increased from 0.25% to 10%.

plot is normalized to the average surface coverage. From these profiles, it is clear that material is more likely to accumulate near the grain boundary at reduced coverage.

To gain insight into the effects of surface coverage and grain boundaries, we carried out Monte Carlo simulations of diffusion-limited cluster–cluster aggregation, DLCCA [24]. The details of the base DLCCA simulation are described in Ref. [12]. The simulation was run on a square lattice with periodic boundary conditions, and the clusters were represented by groups of adjacent occupied cells. Diffusion lengths calculated from the simulation are shown in the inset of Fig. 6 for surface coverages from 0.25% to 10%. As expected, the clusters remained smaller and could diffuse further without coalescing at lower coverage, allowing them to sample more of the buffer surface and be more affected by the grain boundary. When clusters accumulate at the grain boundaries, the local coverage at the center of the grains decreased, allowing clusters at the grain centers to diffuse further. This trend can create the gradient in the surface coverage evident in Figs. 5 and 6.

The ability of the grain boundaries to trap diffusing clusters, combined with the effects of coverage on diffusion length, provides a method for patterning the surface with nanometer size clusters. Clusters can be selectively deposited in the location of grain boundaries and the grain sizes can be controlled, presenting a technique for depositing a size-selected network of particles.

6. Summary

We have demonstrated that the condensation of Xe or Kr on a-C and SiO_x below 40 K results in the formation of polycrystalline films with a mean grain size that weakly increases with condensation temperature. The rare gas forms multilayer islands before covering the surface and, once continuous, the grains grow through secondary growth to form large (1 1 1) oriented grains, independent of the initial number density and the presence of adsorbates on the air exposed substrates. The surface of the film is unstable, and grain boundary grooves that influence BLAG develop at temperatures as low as 20 K. The diffusion of clusters on the film surface during warm-up is affected by the grain boundary grooves. The surface coverage of clusters has a significant effect on diffusion of clusters and capture at the grooves. When the amount of cluster material deposited is small, the grain boundaries can be used to form a web-like pattern of clusters with large cluster-free areas. Knowledge of the buffer structure offers several ways to vary the cluster distribution on the surface and create patterns that can be used to add functionality to surfaces, for example through selective chemisorption or reaction at the clusters.

Acknowledgements

This work was supported in part by the by the US Department of Energy, Division of Materials Sciences under Grant No. DEFG02-01ER45944. The TEM imaging was carried out in the Center for Microanalysis of Materials, University of Illinois, which is partially supported by the US Department of Energy under grant DEFG02-91-

ER45439. ASB is thankful to NSF-INT and the Abdus Salam International Centre for Theoretical Physics for the financial support. We thank S. Sivaramakrishnan for stimulating discussions.

References

[1] P. Jensen, Rev. Mod. Phys. 71 (1999) 1695.
[2] G.D. Waddill, I.M. Vitomirov, C.M. Aldao, J.H. Weaver, Phys. Rev. Lett. 62 (1989) 1568.
[3] L. Huang, S.J. Chey, J.H. Weaver, Phys. Rev. Lett. 80 (1998) 4095.
[4] J.H. Weaver, G.D. Waddill, Science 251 (1991) 1444.
[5] G.D. Waddill, I.M. Vitomirov, C.M. Aldao, S.G. Anderson, C. Capasso, J.H. Weaver, Z. Liliental-Weber, Phys. Rev. B 41 (1990) 5293.
[6] T.R. Ohno, Y.-N. Yang, J.H. Weaver, Y. Kimachi, Y. Hidaka, Appl. Phys. Lett. 57 (1990) 718.
[7] T.R. Ohno, Y.-N. Yang, G.H. Kroll, K. Krause, L.D. Schmidt, J.H. Weaver, Y. Kimachi, Y. Hidaka, S.H. Pan, A.L. de Lozanne, Phys. Rev. B 44 (1991) 2430.
[8] K. Yoo, A.-P. Li, Z.Y. Zhang, H.H. Weitering, F. Flack, M.G. Lagally, J.F. Wendelken, Surf. Sci. 546 (2003) L803.
[9] C.L. Haley, J.H. Weaver, Surf. Sci. 518 (2002) 243.
[10] V.N. Antonov, J.H. Weaver, Surf. Sci. 526 (2003) 97.
[11] V.N. Antonov, J.S. Palmer, A.S. Bhatti, J.H. Weaver, Phys. Rev. B 68 (2003) 205418.
[12] V.N. Antonov, J.S. Palmer, P.S. Waggoner, A.S. Bhatti, J.H. Weaver, Phys. Rev. B 70 (2004) 045406.
[13] P.S. Waggoner, J.S. Palmer, V.N. Antonov, J.H. Weaver, Surf. Sci., in press, doi:10.1016/j.susc.2005.08.020.
[14] G.L. Price, J.A. Venables, Surf. Sci. 49 (1975) 264.
[15] J.F. Hamilton, P.C. Logel, Thin Solid Films 23 (1974) 89.
[16] J.A. Venables, D.J. Ball, J. Cryst. Growth 3 (1968) 180.
[17] C.V. Thompson, Annu. Rev. Mater. Sci. 20 (1990) 245.
[18] C.C. Wong, H.I. Smith, C.V. Thompson, Appl. Phys. Lett. 48 (1985) 335.
[19] J.A. Venables, B.L. Smith, in: M.L. Klein, J.A. Venables (Eds.), Rare Gas Solids, vol. II, Academic, New York, 1977.
[20] C.V. Thompson, J. Appl. Phys. 58 (1985) 763.
[21] W.M. Mullins, J. Appl. Phys. 28 (1957) 333.
[22] M.J. Rost, D.A. Quist, J.W.M. Frenken, Phys. Rev. Lett. 91 (2003) 026101.
[23] Z.G. Xiao, G.A. Rozgonyi, C.A. Canovai, C.M. Osburn, MSR Proc. 202 (1991) 101.
[24] P. Meakin, T. Vicsek, F. Family, Phys. Rev. B 31 (1985) 564.